Nanoscale

ROYAL SOCIETY OF CHEMISTRY

MINIREVIEW

View Article Online
View Journal | View Issue

Cite this: *Nanoscale*, 2025, **17**, 2408

Design strategies and performance enhancements of PVDF-based flexible electrolytes for high-performance all-solid-state lithium metal batteries

Zhongxiu Liu,[a,b,c] Md Shariful Islam,[d] Yuhui Fang,[e] Meifang Zhu,[a] Changyong (Chase) Cao *[d,f] and Guiyin Xu *[a]

Lithium metal is considered one of the most promising anode materials for lithium batteries due to its high theoretical specific capacity (3860 mA h g^{-1}) and low redox potential (−3.04 V). However, uncontrolled lithium dendrite growth and severe interfacial side reactions during cycling result in poor performance and safety risks, significantly limiting its practical applications. Replacing liquid electrolytes with solid polymer electrolytes (SPEs) offers a solution, as SPEs provide flexibility and good electrode compatibility, effectively inhibiting dendrite growth and reducing interfacial reactions. Among SPEs, poly(vinylidene fluoride) (PVDF)-based solid electrolytes offer excellent thermal stability and mechanical strength, making them highly suitable for high-energy-density flexible batteries. This review presents recent advances in PVDF-based solid-state electrolytes (SSEs) for stable, high-performance lithium metal batteries (LMBs). We focus on modification strategies that enhance the performance of PVDF-based SSEs in solid-state LMBs and highlight how synthesis methods, nano/microstructural design, and electrochemical properties are interrelated. Lastly, we discuss the challenges and prospects for PVDF-based SSEs in next-generation high-performance LMBs.

Received 3rd November 2024,
Accepted 23rd December 2024

DOI: 10.1039/d4nr04583a

rsc.li/nanoscale

1. Introduction

Renewable energy sources, including solar, wind, and wave energy, have become increasingly attractive due to the urgency posed by climate change and environmental pollution associated with traditional energy sources.[1–5] However, effectively harnessing these renewable energies remains challenging due to their intermittent and discontinuous nature. Consequently, energy storage devices, particularly rechargeable batteries, are in high demand as they hold substantial potential to mitigate these issues.[6,7] Among various rechargeable batteries, lithium-ion batteries (LIBs) have gained widespread attention for their long life and environmental benefits.[8,9] Nevertheless, commercial LIBs, which use graphite as the anode, have undergone extensive development over the past three decades, nearing their theoretical performance limits and struggling to meet the future demand for high-energy-density storage.[10] Therefore, there is an urgent need to explore new battery systems and materials to achieve higher energy densities.

Compared to commercial lithium-ion batteries, lithium metal batteries (LMBs), which use metallic lithium directly as the anode, offer higher specific energy based on the electroplating and stripping of lithium ions.[11] Lithium metal has an exceptionally high theoretical specific capacity (3860 mA h g^{-1}) and a very low reduction potential (−3.04 V),[12] making LMBs with lithium metal anodes highly promising for achieving high energy densities. Additionally, lithium metal can be used as the anode material directly, eliminating the need for heavy and inactive current collectors, thus further increasing the battery's specific energy.[13] The lithium metal anode (LMA) holds significant potential for development and is highly anticipated as a transformative solution.[14] However, several challenges currently limit its practical application.[15] Firstly, the volume expansion of the lithium metal anode during cycling causes instability in the solid electrolyte interface (SEI) layer, leading to reduced coulombic efficiency and accelerated capacity decay.[16] Secondly, the uncontrolled growth of lithium dendrites can penetrate the separator, causing short circuits, fire hazards, and other safety risks.[17]

[a]*State Key Laboratory for Modification of Chemical Fibers and Polymer Materials, College of Materials Science and Engineering, Donghua University, Shanghai 201620, China. E-mail: xuguiyin@dhu.edu.cn*
[b]*Henan Academy of Sciences, Zhengzhou 450001, China*
[c]*School of Materials Science and Engineering, Zhengzhou University, Zhengzhou 450001, China*
[d]*Laboratory for Soft Machines and Electronics, Department of Mechanical and Aerospace Engineering, Case Western Reserve University, Cleveland, OH 44106, USA. E-mail: ccao@case.edu*
[e]*4D Maker LLC, Okemos, MI 44106, USA*
[f]*Advanced Platform Technology (APT) Center, Louis Stokes Cleveland VA Medical Center, Cleveland, OH 44106, USA*

Organic liquid electrolytes, characterized by high volatility, flammability, and leakage risks, pose inherent safety issues for lithium metal batteries.[18] In contrast, replacing liquid electrolytes with solid-state electrolytes (SSEs) can address these concerns by significantly improving the safety and energy density of lithium metal batteries.[19,20] Solid electrolytes are typically classified as either inorganic or polymer-based.[21–23] Inorganic SSEs offer excellent mechanical properties, thermal stability, and high ionic conductivity,[24] with primary examples including oxides, sulfides, and halides.[25–27] However, large-scale application faces challenges. Although oxide-based SSEs exhibit relatively high ionic conductivity, their rigidity complicates battery processing and assembly and increases interface resistance.[28] During preparation, oxide SSEs often require prolonged high-speed ball milling and elevated temperatures to enhance uniformity and density, resulting in high manufacturing costs. Sulfide and halide SSEs, while having ionic conductivities comparable to liquid electrolytes, generally exhibit narrow electrochemical windows, complicating direct compatibility with high-voltage cathode materials.[28–31]

Polymer-based SSEs, on the other hand, are highly flexible, capable of forming strong interfacial contact with both cathodes and anodes, and exhibit low interfacial impedance, offering significant practical potential.[32] Common polymer substrates include poly(ethylene oxide) (PEO),[33] poly(methyl methacrylate) (PMMA),[34] and poly(vinylidene fluoride) (PVDF).[35] PVDF, a semi-crystalline polymer with radially crystallized, ball-like structures, has chain segments that create a dipole moment due to the presence of electro-negative fluorine and electro-positive hydrogen atoms.[36] This dipole moment grants PVDF a moderate dielectric constant, facilitating the dissociation of lithium salts in the electrolyte. PVDF has various crystalline phases, including α and β phases; α-phase PVDF provides thermodynamic stability, while β-phase offers a higher dielectric constant. PVDF-based SSEs are typically prepared by dissolving PVDF in a solvent, which is then dried and evaporated to form a matrix containing lithium salt.[35] Research by Nan *et al.* has shown that the solvent molecules in the PVDF-based SSE coordinate with lithium ions, facilitating lithium-ion transport by interacting with fluorine atoms on the PVDF chains.[37,38] This ability to promote ionic conductivity has made PVDF-based SSEs attractive for use with lithium metal anodes.

This review will summarize recent advances in PVDF-based flexible SSEs for lithium metal batteries, focusing on modification strategies, electrochemical performance, and design structures. We will also discuss the preparation and modification methods, the nano- and microstructures, and the electrochemical properties of PVDF-based SSEs. Finally, we will provide an outlook on the potential of PVDF-based SSEs for high-performance lithium metal batteries.

2. Design strategies and properties of PVDF-based flexible SSEs in LMBs

PVDF exhibits several ideal properties for fabricating solid-state electrolytes,[35] including (1) high mechanical strength and toughness, (2) a wide electrochemical voltage window, (3) excellent thermal stability – capable of sustained operation at temperatures up to 150 °C with a decomposition threshold around 400 °C, and (4) high electrochemical stability with minimal reactive interference with other materials. These properties contribute to PVDF's ability to dissociate lithium more efficiently due to its high dielectric constant, which reduces interactions between ion pairs and facilitates ion transport. With a relative permittivity of 8.3,[35] PVDF supports a favorable

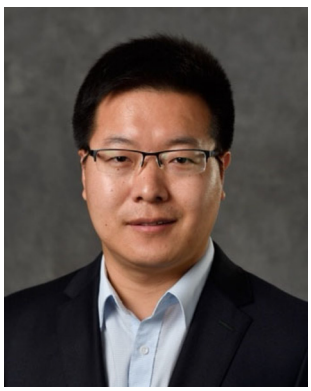

Changyong (Chase) Cao

Dr Changyong (Chase) Cao is an Assistant Professor in the Departments of Mechanical and Aerospace Engineering, and Electrical, Computer, and Systems Engineering at Case Western Reserve University (CWRU). He also serves as an Investigator at the Advanced Platform Technology (APT) Center of the Louis Stokes Cleveland VA Medical Center. Dr Cao earned his Ph.D. in Mechanical Engineering and Materials Science from the Australian National University and completed postdoctoral training at Duke University. His research focuses on flexible and stretchable electronics, soft robotics, energy harvesting and storage, multifunctional materials, and 3D/4D printing.

Guiyin Xu

Dr Guiyin Xu received a PhD degree from Nanjing University of Aeronautics and Astronautics in 2017. He is currently a processor at the State Key Laboratory for Modification of Chemical Fibers and Polymer Materials, College of Material Science and Engineering, Donghua University. Before that, he worked as a postdoctor at Massachusetts Institute of Technology from 2018 to 2021. His research interest is the application of functional fiber membranes in green energy and environmental restoration.

environment for lithium dissociation, aiding in the overall ionic conductivity of the SSE.

By leveraging these intrinsic PVDF properties, researchers have developed various modification techniques to engineer polymer electrolytes with enhanced and consistent performance. Key strategies for optimizing PVDF-based SSEs in LMBs include:

Doping with inorganic fillers: Incorporating inorganic fillers such as Li_3PO_4, Al_2O_3, or LLZTO improves ionic conductivity, mechanical strength, and stability. These fillers help reduce crystallinity in PVDF, creating more amorphous regions that facilitate lithium-ion mobility and improve electrochemical performance.

Blending with organic fillers: Organic additives like poly (ethylene oxide) (PEO) or poly(methyl methacrylate) (PMMA) can be blended with PVDF to increase flexibility, reduce brittleness, and improve interface compatibility with lithium metal anodes. Blending polymers also adjusts the mechanical properties, enhancing stability during battery cycling.

Inorganic/organic composite fillers: A combined approach using both inorganic and organic fillers can yield synergistic benefits, where inorganic components contribute to thermal stability and ionic conductivity, while organic additives enhance flexibility and interfacial contact with electrodes.

Chemical modification of PVDF: Chemical modifications such as grafting and functionalizing PVDF with ion-conducting groups can increase its ionic conductivity by introducing additional lithium-ion conduction pathways and lowering the glass transition temperature.

These modification strategies, outlined in Scheme 1, facilitate the design of PVDF-based SSEs that meet the specific requirements of high-performance LMBs. Table 1 summarizes the synthesis methods, compositions, and electrochemical properties of various PVDF-based SSEs tailored for LMB applications. By systematically exploring and combining these approaches, PVDF-based electrolytes can achieve the high stability, flexibility, and ionic conductivity necessary for advanced LMB technologies.

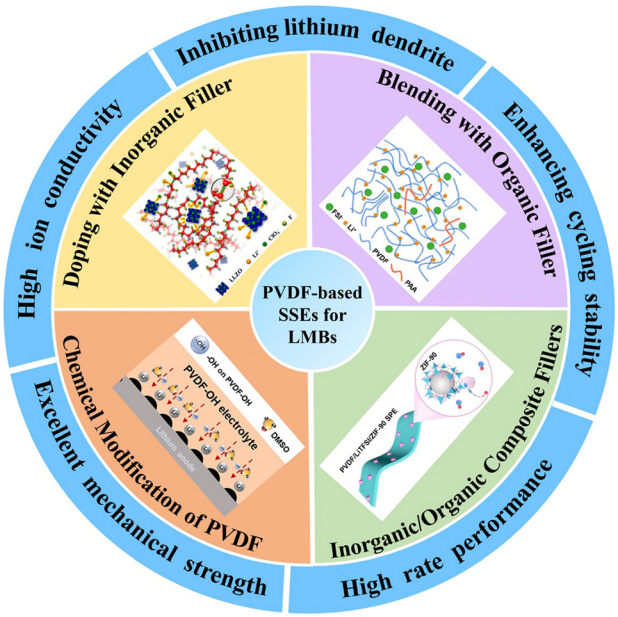

Scheme 1 Design strategies and properties of PVDF-based flexible electrolytes for high-performance all solid-state Lithium Metal Batteries (LMBs).

2.1 Doping with inorganic fillers

One of the most common enhancement strategies for PVDF-based solid-state electrolytes (SSEs) is doping with inorganic fillers. These fillers typically come in three morphological forms: zero-dimensional (0D) nanoparticles, one-dimensional (1D) nanowires, and two-dimensional (2D) nanosheets. These active fillers act as ion carriers and participate in lithium-ion (Li^+) conduction, promoting efficient ion transfer and enhancing the electrolyte's ionic conductivity. Additionally, the free volume spaces generated at the interfaces between ceramic fillers and the PVDF matrix provide additional ion transport pathways. Consequently, introducing active fillers to boost the ionic conductivity of PVDF-based SSEs has gained substantial interest in recent years.

For instance, Nan *et al.* developed composite solid electrolytes (CSEs) with garnet-type $Li_{6.75}La_3Zr_{1.75}Ta_{0.25}O_{12}$ (LLZTO) nanoparticles as active fillers.[39] The La atoms in LLZTO interact with nitrogen atoms and C═O groups from the solvent *N*,*N*-dimethylformamide (DMF), creating electron-enriched nitrogen atoms that act as Lewis bases, leading to the dehydrofluorination of PVDF. This interaction between PVDF, lithium salt, and LLZTO enhances the flexible electrolyte's performance, resulting in a high ionic conductivity of approximately 0.5 mS cm^{-1} at 25 °C. In a similar study, Liu *et al.* fabricated flexible CSEs using a PVDF matrix with lithium salt (LiTFSI), DMF, and NASICON-type $Li_{1.3}Al_{0.3}Ti_{1.7}(PO_4)_3$ (LATP) ceramic nanoparticles as fillers.[40] DMF facilitates lithium salt dissociation and forms lithium-rich complexes $[Li(DMF)_nTFSI]$ with Li^+, which exhibit ionic liquid-like characteristics that improve conductivity. This design yielded a LATP-PVDF/Li CSE with a high ionic conductivity of 0.244 mS cm^{-1} and an electrochemical stability window of up to 4.8 V (*vs.* Li^+/Li).

However, the thickness and limited mechanical strength of PVDF-based SSEs can restrict their practical applications. To address this, Ma *et al.* developed an ultrathin PVDF-based SSE by integrating a 7 μm polyethylene (PE) separator and SiO_2 nanoparticles with silicon hydroxyl (Si-OH) groups.[41] This composite, known as PPSE, achieved a total thickness of only 20 μm and exhibited ultra-high mechanical strength (64 MPa). The nano-SiO_2 particles anchored DMF molecules, enhancing ion conductivity in PVDF and preventing side reactions with lithium metal. This modification increased the ionic conductivity to 0.48 mS cm^{-1}, reduced activation energy (0.19 eV), and achieved a high lithium transference number (0.59).

Introducing functional fillers with ferroelectric or dielectric properties has also proven effective in improving PVDF-based SSEs. For instance, Kang *et al.* utilized dielectric $NaNbO_3$ nanoparticles in a PVDF-based SSE (PNNO-5), which induced

Table 1 Summary of synthesis methods and performance of PVDF-based solid-state lithium metal batteries (SSLMBs)

Electrolyte	Synthetic methods	σ^a (mS cm^{-1})	$t_{Li^+}{}^b$	LSV[c] (V)	MS[d] (MPa)	Lifespan T^e h [$F_1{}^f$ (mA cm^{-2}), $F_2{}^f$ (mA h cm^{-2})]	Battery configuration	Performance	Ref.
Inorganic filler									
Nanoparticles									
PVDF/$LiClO_4$/DMF/$Li_{6.75}La_3Zr_{1.75}Ta_{0.25}O_{12}$	Solution-casting method	0.5	—	—	5.92	160 (0.05, 0.025)	$LiCoO_2$/Li	150, 98% (120 cycles, 0.4C)	39
PVDF/LiTFSI/DMF/$Li_{1.3}Al_{0.3}Ti_{1.7}(PO_4)_3$	Solution-casting method	0.244	0.52	4.8	—	3000 (0.1)	$LiNi_{0.6}Co_{0.2}Mn_{0.2}O_2$/Li	125, 80% (400 cycles, 0.5C)	40
PVDF/LiFSI/DMF/SiO_2	Solution-casting method	0.481	0.59	—	64	11 000 (0.1, 0.1)	$LiNi_{0.8}Mn_{0.1}Co_{0.1}O_2$/Li	173, (300 cycles, 0.5C)	41
PVDF/LiFSI/DMF $NaNbO_3$	Solution-casting method	0.556	0.49	4.7	—	2800 (0.1, 0.1)	$LiNi_{0.8}Mn_{0.1}Co_{0.1}O_2$/Li	177, 67.7% (1500 cycles, 1C)	42
PVDF/LiTFSI/DMF/$BiFeO_3$	Casting and scraping method	0.139	0.35	4.7	—	2500 (0.1, 0.1)	$LiNi_{0.8}Mn_{0.1}Co_{0.1}O_2$/Li	141.7, 89% (400 cycles, 0.3C)	43
PVDF/LiTFSI/NMP/$LiSnZr(PO_4)_3$	Solution-casting method	0.0576	0.73	4.73	—	2000 (0.04)	$Li_4Ti_5O_{15}$/Li	133, 88% (20, 0.1C)	44
PVDF/LiTFSI/DMF/$Li_3Zr_2Si_2PO_{12}$	Solution-casting method	0.228	—	5.2	—	600 (0.1)	$LiNi_{0.5}Co_{0.2}Mn_{0.3}O_2$/Li	150, 88.5% (100 cycles, 0.1C)	45
PVDF/LiFSI/DMF/$Li_{6.5}La_3Zr_{1.5}Ta_{0.1}Nb_{0.4}O_{12}$	Solution-casting method	0.105	0.66	4.8	—	400 (0.1, 0.1)	$LiNi_{0.8}Mn_{0.1}Co_{0.1}O_2$/Li	137, (80 cycles, 0.3C)	46
PVDF/LiTFSI/DMF/$LiNO_3$	Solution-casting method	0.129	0.32	—	—	400 (0.2, 0.2)	$LiNi_{0.8}Mn_{0.1}Co_{0.1}O_2$/Li	118.5, 93% (200 cycles, 0.5C)	47
PVDF/LiFSI/DMF/MS zeolite	Solution-casting method	0.45	0.47	4.6	—	5100 (0.1, 0.1)	$LiNi_{0.8}Mn_{0.1}Co_{0.1}O_2$/Li	178.5, 92.7% (500 cycles, 1C)	48
PVDF/$LiClO_4$/DMF/$(Mg,Al)_2Si_4O_{10}(OH)$	Casting and scraping method	0.12	0.54	—	4.7	100 (0.05, 0.05)	$Ni_{1/3}Mn_{1/3}CO_{1/3}O_2$/Li	117.6, 97% (200 cycles, 0.3C)	49
Nanowire									
PVDF/LiTFSI/NMP/$Li_{0.35}La_{0.55}TiO_3$	Solution-casting method	0.53	—	5.1	9.5	300 (0.2, 0.2)	$LiFePO_4$/Li	121, 99% (100 cycles, 1C)	50
PVDF/LiFSI/DMF-$BaTiO_3$/$Li_{0.33}La_{0.56}TiO_{3-x}$	Solution-casting method	0.82	0.57	—	2.11	1900 (0.1, 0.1)	$LiNi_{0.8}Mn_{0.1}Co_{0.1}O_2$/Li	180, 70% (1000 cycles, 1C)	51
PVDF/$LiClO_4$/DMF/V_2O_5	Solution-casting method	2.2	0.58	5.2	—	2500 (0.5, 0.5)	$LiFePO_4$/Li	150, 95.3% (300 cycles, 0.1C)	52
PVDF/LiTFSI/DMF/d-HNTs	Casting and scraping method	0.29	0.75	—	49	400 (0.5, 0.5)	$LiFePO_4$/ $LiLiNi_{0.8}Mn_{0.1}Co_{0.1}O_2$/Li	148, 80% (300 cycles, 1C) 149, 70% (200 cycles, 1C)	53
PVDF/LiTFSI/DMF/LiF/LLAZO	Casting and scraping method	0.44	0.33	4.9	—	300 (0.1, 0.1)	$LiFePO_4$/Li	167, 96% (250 cycles, 0.5C)	54
Nanosheet									
PVDF/LiFSI/DMF/g-C_3N_4	Solution-casting method	0.69	0.49	4.7	11.2	2200 (0.1, 0.1)	$LiNi_{0.8}Mn_{0.1}Co_{0.1}O_2$/Li	146.5, 76.6% (1700 cycles, 1C)	55
PVDF/LiODFB/DMF/PC	Casting and scraping method	0.118	—	4.75	4.3	160 (0.1, 0.1)	$LiCoO_2$/Li	125, 84% (300cycles, 0.1C)	56
PVDF/LiTFSI/NMP/ISMN	Solution-casting method	0.44	0.5	4.92	—	5000 (0.2, 0.1)	$LiFePO_4$/Li	154, 88.9% (500 cycles, 0.5C)	57
PVDF/LiTFSI/NMP/h-BN	Solution-casting method	0.29	0.62	5.24	3.45	1200 (0.1, 0.1)	$LiFePO_4$/Li	121.4, 96% (160 cycles, 0.2C)	58

Table 1 *(Contd.)*

Electrolyte	Synthetic methods	σ^a (mS cm^{-1})	t_{Li^+} [b]	LSV[c] (V)	MS[d] (MPa)	Lifespan T^e h [F_1 [f] (mA cm^{-2}), F_2 [f] (mA h cm^{-2})]	Battery configuration	Performance	Ref.
Organic filler									
PVDF/LiFSI/DMF/PAA	Solution-casting method	0.09	—	4.64	—	900 (0.44, 0.22)	$LiCoO_2$/Li	125, 97% (1000 cycles, 0.1C)	59
PVDF/LiTFSI/DMSO/AMPS	Solution-casting method	0.22	0.49	4.7	—	2100 (0.1, 0.1)	$LiFePO_4$/Li	127.6, 90.8% (220 cycles, 1C)	60
PVDF/LiTFSI/DMF/TFBQ	Solution-casting method	0.239	0.42	5.0	—	2000 (0.1, 0.1)	$LiNi_{0.6}Co_{0.2}Mn_{0.2}O_2$/Li	150, 80% (180 cycles, 0.2C)	61
PVDF/LiTFSI/DMF/MgPFPAA	Casting and scraping method	0.14	0.34	4.8	—	2400 (0.2, 0.2)	$LiFePO_4$/Li	120, 74.9% (1500 cycles, 5C)	62
PVDF/LiTFSI/DMF/HFA	Casting and scraping method	0.241	—	4.9	—	1700 (0.1, 0.1)	$LiNi_{0.6}Co_{0.2}Mn_{0.2}O_2$/Li	176.8, 80% (600 cycles, 0.2C)	63
PVDF/LiFSI/DMF/FEC/LIDFP	Solution-casting method	0.479	0.43	4.6	6.5	3000 (0.1, 0.1)	$LiFePO_4$/Li	148, 84% (400 cycles, 1C)	64
Organic/inorganic filler									
PVDF/LiFSI/DMF-h-PAN@MOF	Solution-casting method	1.03	—	4.45	20.8	3200 (0.1, 0.1)	$LiNi_{0.8}Mn_{0.1}Co_{0.1}O_2$/Li	150, 61.9% (1400 cycles, 2C)	65
PVDF/PVAC/LiTFSI/LiBOB/DMF/$Li_{6.4}La_3Zr_{1.4}Ta_{0.6}O_{12}$	Casting and scraping method	0.496	0.57	5.4	6	1300 (0.1, 0.1)	$LiFePO_4$/Li	145, 92.3% (220 cycles, 0.5C)	66
PVDF/LiTFSI/NMP/ZIF-90	Casting and scraping method	0.62	0.48	—	2.1	1000 (0.05, 0.05)	$LiFePO_4$/Li	120, 95% (300 cycles, 1C)	67
Other strategy									
PVDF-OH/LiTFSI/DMSO	Solution-casting method	0.71	—	—	16.1	1000 (0.1, 0.1)	$LiFePO_4$/Li	145.9, 85.4% (1000 cycles, 0.5C)	68
P(VDF-CHF_3-CH_2FCl)/LiFSI/DMF	Solution-casting method	0.78	0.57	4.4	—	11 000 (0.05, 0.05)	$LiNi_{0.8}Mn_{0.1}Co_{0.1}O_2$/Li	154, 94.9% (300 cycles, 1C)	69
PVDF/LiTFSI/NMP/$Li_{6.1}Al_{0.3}La_3Zr_2O_{12}$ framework	Immersing method	0.437	0.72	5.08	—	1000 (0.1, 0.1)	$LiNi_{0.6}Co_{0.2}Mn_{0.2}O_2$/Li	160, 90% (200 cycles, 0.2C)	70
PVDF741/$LiClO_4$/DMF	Casting and scraping method	0.12	—	4.9	—	1000 (0.1, 0.1)	$LiFePO_4$/Li	100, 80% (500 cycles, 0.5C)	71
P(VDF-TrFE-CTFE)/LiTFSI/DMF	Solution-casting method	0.31	0.33	4.6	—	1200 (0.05, 0.05)	$LiFePO_4$/Li	146, 98.5% (150 cycles, 0.5C)	72

[a] Conductivity (room temperature). [b] Ion transference number. [c] Linear sweep voltammetry testing electrochemical stability. [d] Mechanical strength. [e] Time (h). [f] F_1: current density (mA cm^{-2}); F_2: specific area capacity (mA h cm^{-2}).

the formation of a high-dielectric β-phase in PVDF (Fig. 1a).[42] This phase enhances Li^+ coordination with FSI^- anions due to polarized F atoms, which aid in abundant and mobile Li^+ ion formation (Fig. 1b–d). The PNNO-5 SSE achieved a high ionic conductivity of 0.556 mS cm^{-1}, with a decreased ion migration activation energy of 0.22 eV, as compared to 0.33 eV in unmodified PVDF SSEs (Fig. 1e). This configuration allowed a $LiNi_{0.8}Mn_{0.1}Co_{0.1}O_2$ (NCM811)/PNNO-5/Li cell to retain 67.7% capacity over 1500 cycles at 1C and demonstrated a high initial capacity of 177.2 mA h g^{-1} with 95% retention over 100 cycles at 0.5C (Fig. 1f).

Li *et al.* also introduced ferroelectric $BiFeO_3$ nanoparticles to modify PVDF-based SSEs, which helped distribute the electric field more uniformly at the electrolyte/electrode interface,

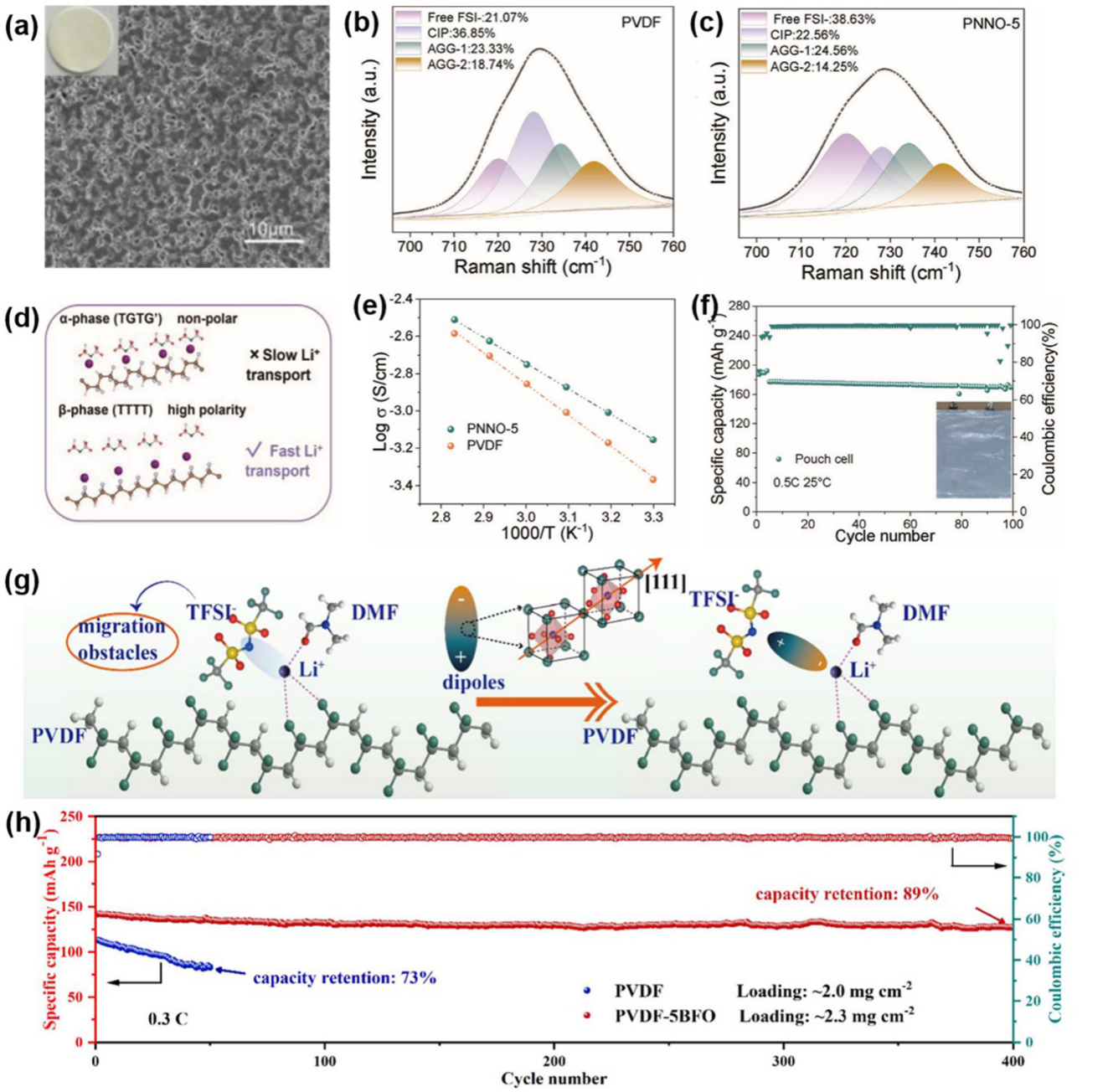

Fig. 1 Introducing functional fillers with ferroelectric or dielectric properties to improve PVDF-based SSEs. (a) Surface SEM images and optical photographs of PNNO-5. (b and c) Raman spectra of PVDF and PNNO-5. (d) Schematic illustration showing Li salt dissociation facilitated by the β-phase of PVDF. (e) Arrhenius plots comparing ionic conductivity of PVDF and PNNO-5 electrolytes. (f) Cycling performance of NCM811/PNNO-5/Li pouch cell. Reproduced with permission.[42] Copyright 2024, Advanced Materials. (g) Schematic illustration of the dipole effect on the conduction mechanism. (h) Cycling performance of Li/NCM811 batteries. Reproduced with permission.[43] Copyright 2024, Journal of Materials Chemistry A.

resulting in uniform Li deposition.[43] The transference number of Li^+ increased from 0.18 to 0.35 compared to pure PVDF, enhancing overall battery performance. The $BiFeO_3$ particles' spontaneous polarization along the [111] direction generates dipoles that interact electrostatically with $TFSI^-$ anions (Fig. 1g), further dissociating LiTFSI and reducing the migration resistance of $[Li(DMF)_x]^+$ complexes. The assembled Li/NCM811 full cells showed an excellent performance, which a high coulombic efficiency of 99% and a capacity retention of 89% achieved after 400 cycles (Fig. 1h).

Compared to granular fillers, ceramic nanowires can substantially enhance the conductivity of SSEs by creating continuous pathways that facilitate lithium-ion transport. The interconnected nanowire network also improves the electrolyte's mechanical strength, thus enhancing battery stability and safety.[73] For instance, Su and colleagues developed a CSE with $Li_{0.35}La_{0.55}TiO_3$ nanofibers and PVDF/LiTFSI, achieving an ionic conductivity of 0.53 mS cm^{-1} at room temperature and a voltage window up to 5.1 V.[50] Shi *et al.* synthesized $BaTiO_3$-$Li_{0.33}La_{0.56}TiO_{3-x}$ (BTO-LLTO) nanowires with a heterojunction structure through electrospinning, followed by calcination at 1000 °C.[74] Introducing these nanowires into a PVDF matrix yielded a PVDF-based CSE (PVBL) with high ionic conductivity (0.82 mS cm^{-1}) and lithium transference number (0.57) (Fig. 2a–c). The PVBL exhibited stable cycling for over 1900 hours at 0.1 mA cm^{-2} and 0.1 mA h cm^{-2} in a symmetrical cell (Fig. 2d) and achieved a capacity retention of 70% after 1000 cycles in an NCM811/PVBL/Li battery (Fig. 2e).

In another study, He *et al.* incorporated g-C_3N_4 nanosheets (GCNs) into a PVDF-based SSE, achieving high ionic conductivity of 0.69 mS cm^{-1}.[75] During cycling, GCNs react with lithium metal to form a Li_3N-enriched SEI layer, significantly reducing side reactions and ensuring rapid charge transfer. The GCNs' adsorption capacity for residual DMF further improves electrochemical stability, enabling the Li symmetrical cell to cycle steadily for 2200 hours at 0.1 mA cm^{-2} and 0.1 mA h cm^{-2}. Additionally, the NCM811 cathode-based LMBs exhibited a high discharge capacity of 108 mA h g^{-1} at 5C and excellent cycling stability over 1700 cycles at 1C.

In summary, doping PVDF-based SSEs with various inorganic fillers – ranging from 0D nanoparticles to 1D nanowires and 2D nanosheets – enhances their electrochemical properties by increasing ionic conductivity, mechanical strength, and stability, facilitating promising applications in high-performance lithium metal batteries.

2.2 Blending with organic fillers

PVDF-based SSEs are often prepared by solution casting using DMF as a solvent, which results in the formation of a [DMF-Li^+] complex that improves Li^+ transport. However, residual DMF can react with lithium metal over time, compromising the interface between the PVDF-based SSE and Li anode. To address this, Nan *et al.* introduced propylene carbonate (PC) into PVDF-based SSEs to stabilize the interface between the SSE and Li anode by controlling the solvation structure.[56] PC accelerates the dissociation of lithium oxalyldifluoroborate (LiODFB), forming a robust interfacial layer of "lithium propylene decarbonate (LPDC)–B–O" oligomers. This dense, uniform layer enhances contact and suppresses continuous reactions between residual DMF and the Li anode, achieving a high ionic conductivity of 1.18 mS cm^{-1}. The resulting $LiCoO_2$/Li full batteries deliver 139.2 mA h g^{-1}, retaining 84% of capacity after 300 cycles at 0.1C.

To further stabilize the interface, Zhang *et al.* incorporated isosorbide mononitrate (ISMN), a functional additive with a non-resonant structure (O_2–N–O–), into PVDF-based SSEs to create a stable N-rich solid electrolyte interface, reducing Li dendrite formation and side reactions (Fig. 3a).[57] ISMN, when added to PVDF-based SSEs, forms a stable interface upon lithium stripping/plating by cleaving the N–O bond in its non-resonant structure, yielding a nitrogen-rich layer that enhances ultra-stable flexible SSLMBs. The Li/Li symmetric cell achieved stable Li stripping/plating cycling for over 5000 hours at a current density of 0.2 mA cm^{-2} and capacity of 1.0 mA h cm^{-2}. Additionally, the Li|$LiFePO_4$ cell exhibited an initial discharge capacity of 154.0 mA h g^{-1}, with a capacity retention of 88.9% after 500 cycles at 0.5C. The flexible NCM622/Li pouch cell maintained a high discharge capacity retention of 97.2% over 100 cycles at 0.5C.

Moreover, Nan *et al.* developed a PVDF-based SSE with 2-acrylamido-2-methylpropane sulfonic acid (AMPS) as an additive to enhance Li^+ conduction by reducing the crystallinity of PVDF and immobilizing anions.[60] AMPS induces the formation of a LiF/Li_2S_x/Li_2SO_3/Li_3N-rich interface at the Li anode, suppressing dendrite growth (Fig. 3b–d). The resulting AMPS-PVDF polymer electrolyte (AP-PE) enables symmetric cells to cycle stably for 2100 hours at 0.1 mA cm^{-2} and 0.1 mA h cm^{-2}. After 500 hours of cycling, the Li anode in these symmetric cells exhibited a clean surface with no dendrite formation (Fig. 3e). The Li/AP-PE/LFP cell demonstrated stable cycling performance, retaining 90.8% of its capacity after 200 cycles at 0.5C (Fig. 3e–g).

By blending PVDF-based SSEs with various organic fillers, researchers have significantly enhanced ionic conductivity, interface stability, and cycling performance, making these electrolytes viable candidates for high-performance, long-lasting LMBs.

2.3 Inorganic/organic composite fillers

In PVDF-based SSEs, porous structures can lead to disordered ion flux and reduced mechanical strength, resulting in non-uniform lithium deposition and promoting lithium dendrite growth (Fig. 4a). To address this, Ma *et al.* designed a composite filler by incorporating interconnected metal–organic framework (MOF)-coated heat-treated polyacrylonitrile (h-PAN@MOF) fiber networks into a PVDF matrix, creating composite SSEs termed PPM (Fig. 4b). The MOF (UIO-66NH_2) particles on the PAN fibers interact strongly with the C=O groups of DMF molecules, weakening the Li^+–O bond strength in DMF and facilitating Li^+ transport along the h-PAN@MOF networks. This design achieved a high ionic conductivity of 1.03 mS cm^{-1} (Fig. 4a).

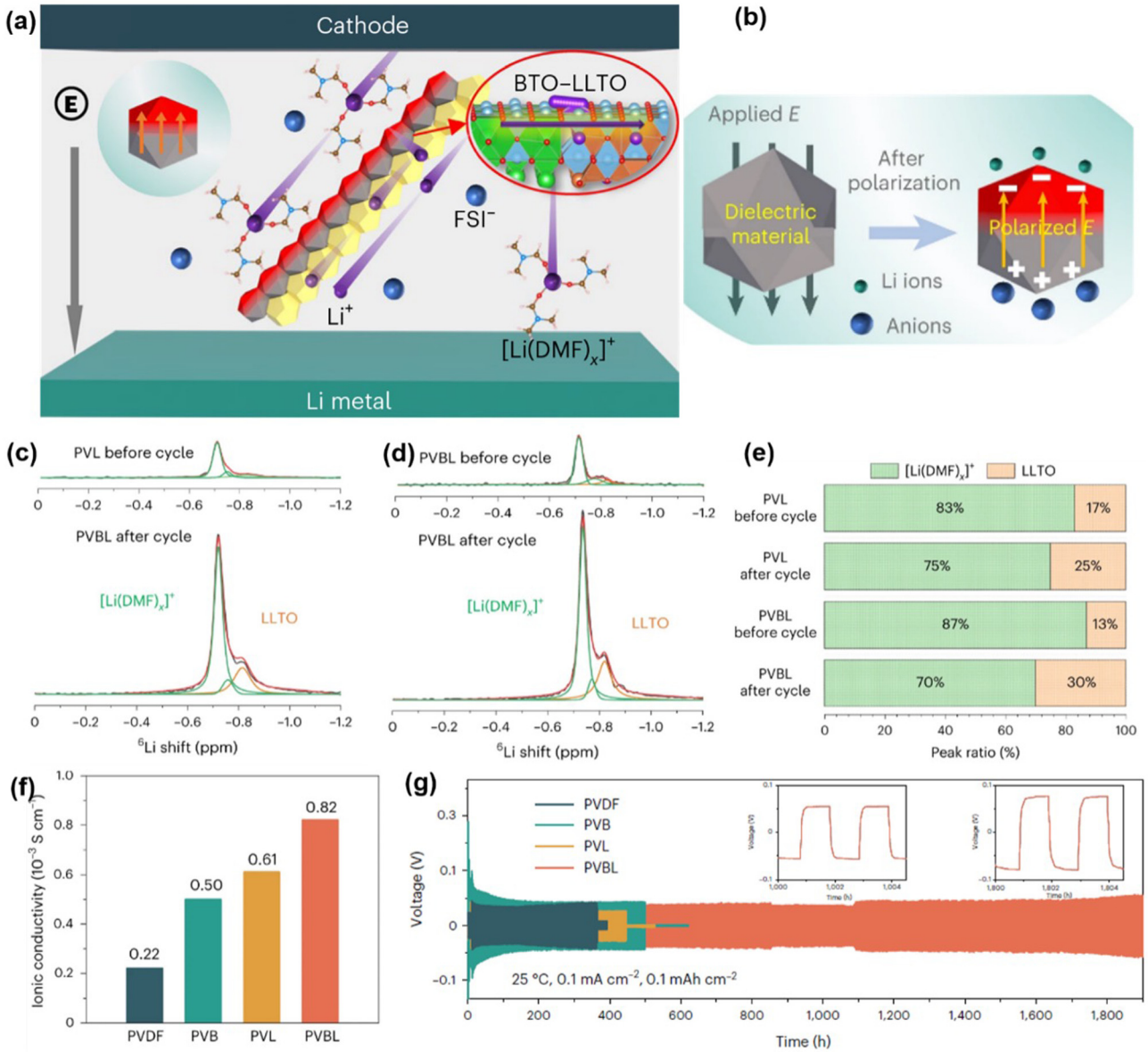

Fig. 2 Incorporating an interconnected nanowire network to enhance PVDF-based SSEs. (a) Illustration of the Li salt dissociation and Li^+ transport facilitated by the coupled BTO-LLTO in the PVBL electrolyte. (b) Schematic of Li salt dissociation by a polarized dielectric material. (c) The ssNMR spectra of the PVL and (d) PVBL electrolytes before and after cycling in a ^6Li symmetric cell, with (e) corresponding peak ratios of $^6Li^+$ transport paths. (f) Ionic conductivities of the PVDF-based electrolytes at 25 °C. (g) Long-term cycling performance of PVBL in symmetric cells. Reproduced with permission.[51] Copyright 2017, Nature Nanotechnology, Nature Publishing Group.

The h-PAN@MOF network also imparts high mechanical strength (20.84 MPa) to the electrolyte, effectively inhibiting lithium dendrite growth. The adsorption energy of the C=O group in DMF on the MOF crystal (−1.11 eV) is three times greater than that on the PVDF chains (−0.35 eV). This strong adsorptive interaction between DMF and MOF realigns solvent molecules around the h-PAN@MOF networks, significantly reducing DMF decomposition at the PPM electrolyte/lithium metal interface.

Solid-state nuclear magnetic resonance (ss-NMR) spectroscopy of the ^7Li and ^{19}F spectra was conducted to examine the interactions between FSI-Li^+ and DMF-Li^+ complexes. An upfield shift in the ^7Li spectrum indicates an enhanced shielding effect of lithium nuclei in the PPM electrolyte, suggesting tighter coordination with surrounding ligands (Fig. 4c). Changes in chemical shifts in the ^{19}F spectra of FSI also indicate a weakened DMF-Li^+ interaction and stronger FSI-Li^+ coordination (Fig. 4d). The combined effects of h-PAN and MOF establish a competitive Li^+ coordination environment and alter solvation structures to promote rapid, linear Li^+ transport. This synergy enhances interfacial stability with electrodes.

As a result, the Li|PPM|Li battery demonstrated stable voltage hysteresis over 3200 hours at a current density of

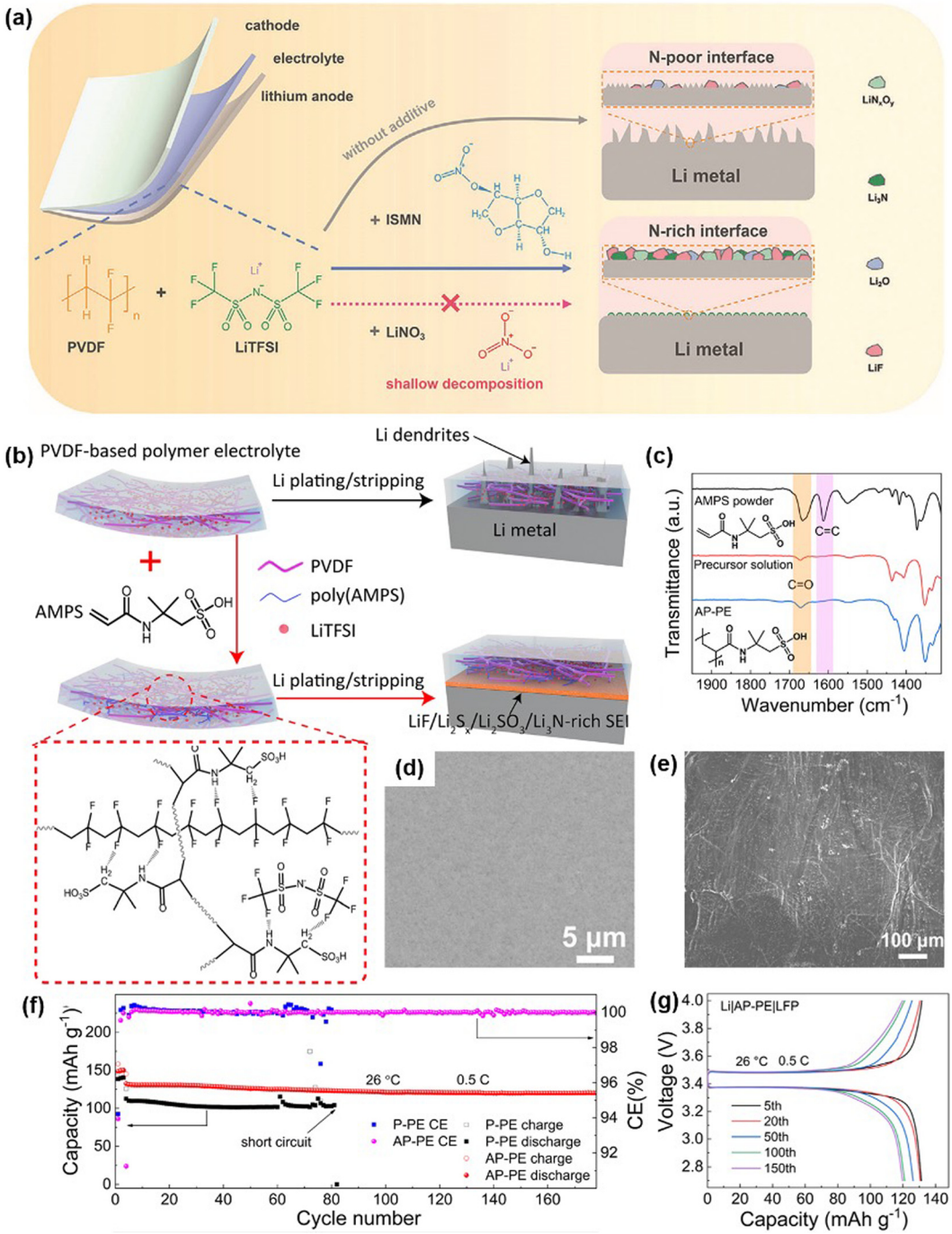

Fig. 3 Enhancing PVDF-based SSE through blending with organic fillers. (a) Schematic illustration of the modification mechanism using ISMN for PVDF-based SSE. Reproduced with permission.[57] Copyright 2024, Advanced Functional Materials. (b) Schematic illustration showing the role of AMPS in promoting Li^+ conduction and suppressing Li dendrite formation. (c) FTIR spectra of AP-PE. (d) SEM images of the AP-PE membrane. (e) SEM images of Li electrodes from Li/AP-PE after 500 hours of cycling at 0.1 mA cm^{-2} and 0.1 mA h cm^{-2}. (f) Cycling performance of Li/AP-PE/LFP batteries at 0.5C and (g) the corresponding charge–discharge voltage profiles. Reproduced with permission.[60] Royal Society of Chemistry 2022.

0.1 mA cm^{-2} and a capacity of 0.1 mA h cm^{-2} (Fig. 4e). Additionally, the Li|PPM|NCM811 battery retained 61.9% of its capacity over 1400 cycles at 2C (Fig. 4f). This promising performance highlights the effectiveness of inorganic/organic composite fillers in enhancing the stability and ionic conductivity of PVDF-based SSEs in lithium metal batteries.

2.4 Chemical modification of PVDF

Beyond doping fillers and blending with polymers, direct modification of PVDF is an effective method to enhance the performance of PVDF-based SSEs. For example, Zeng *et al.* modified PVDF by introducing –OH groups into the PVDF

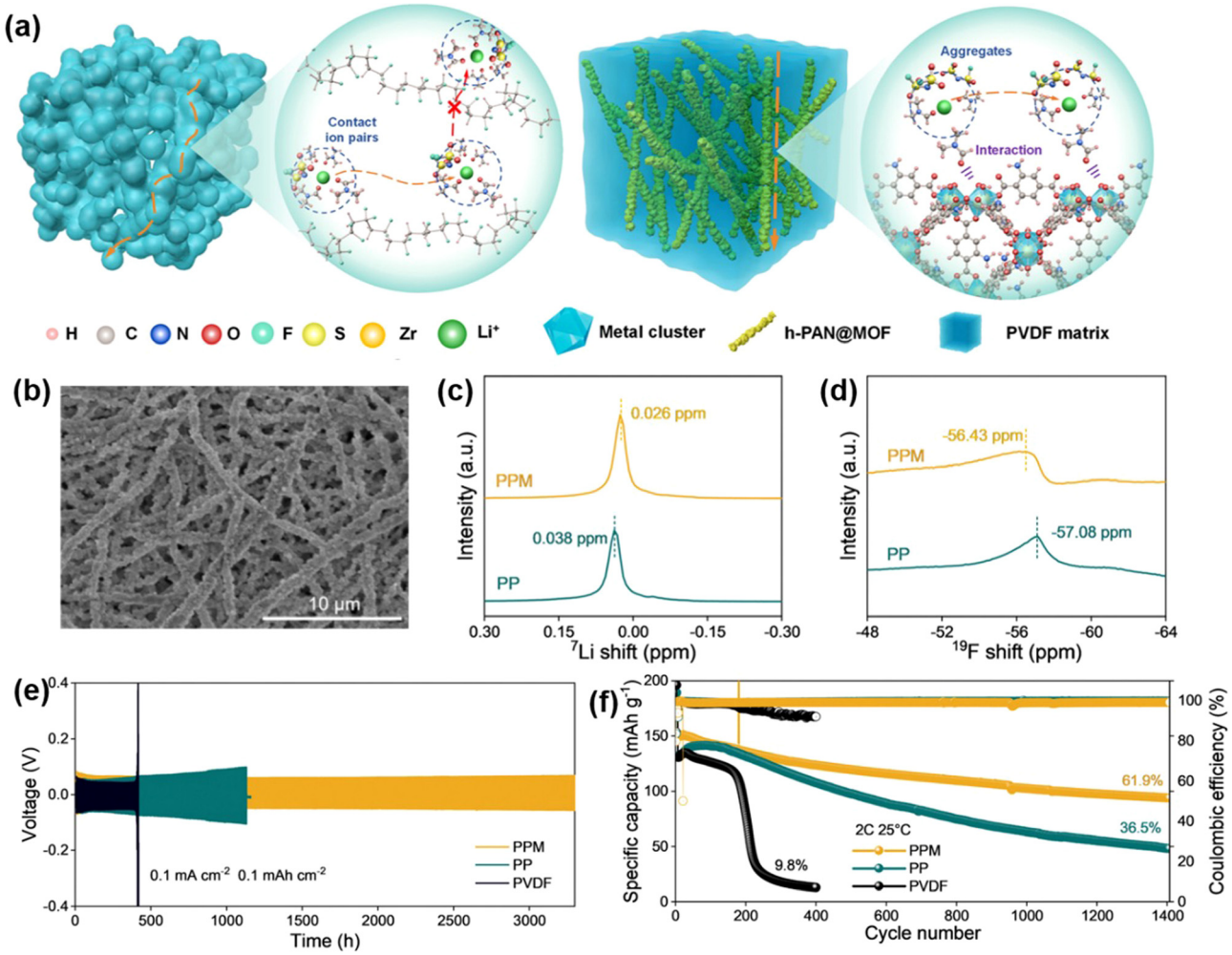

Fig. 4 Inorganic/organic composite fillers for enhanced PVDF-based SSE. (a) Schematic of ion transport and solvation structures in PVDF and PPM electrolytes. (b) SEM images of h-PAN@MOF networks. (c) ^{7}Li ss-NMR spectra. (d) ^{19}F ss-NMR spectra. (e) Galvanostatic cycling curves of Li||Li symmetric cells with PVDF, PP, and PPM electrolytes. (f) Long-term cycling stability of Li||NCM811 cells. Reproduced with permission.[51] Copyright 2023, Nature Nanotechnology, Nature Publishing Group.

chain segments.[68] By applying molecular anchoring principles, the typically disordered DMSO molecules within PVDF align through hydrogen bonding, creating an efficient pathway for rapid Li^+ transport. The resulting LFP|PVDF–OH|Li battery achieved an initial capacity of 145.9 mA h g^{-1} at 0.5C, with a capacity retention of 85.4% after 1000 cycles. Additionally, the PVDF–OH SSE in an LFP|Li pouch battery delivered an initial capacity of 124.47 mA h g^{-1}, retaining 98% of its capacity after 200 cycles at 0.5C.

In another advancement, Huang *et al.* demonstrated that Li^+ can transport through the crystalline phase of PVDF by incorporating dipolar defects into the crystals.[69] By adding trifluoroethylene (CHF_3) and chlorofluoroethylene (CH_2FCl) as dipolar defects into VDF crystals, they triggered rapid Li^+ movement through ion–dipole interactions. These defects expanded the interchain distance in PVDF from 4.39 to 4.83 Å, facilitating $-CH_2CF_2$ dipole vibrations at room temperature and supporting Li^+ migration through ion-dipole interactions, thereby transforming PVDF into a fast ion conductor (Fig. 5a). As a result, the defective PVDF (d-PVDF) SSE achieved a high ionic conductivity of 0.78 mS cm^{-1} and a lithium-ion transference number (t_{Li^+}) of 0.57 (Fig. 5d).

Further analysis with displacement-electric field (D–E) measurements showed that d-PVDF, unlike ferroelectric (FE) PVDF, exhibited a slim hysteresis loop, indicating a significant reduction in coercive field from 67.3 to 10.7 MV m^{-1} (Fig. 5b). This observation confirmed the presence of $-CHF_3$ and $-CH_2FCl$ dipolar defects in the VDF crystals, which promote Li^+ integration within the crystals, transforming defective d-PVDF crystals into single-ion conductors (Fig. 5c). The Li/d-PVDF/Li symmetrical cell demonstrated an extended lifespan of 11 000 hours (450 days) at 0.05 mA cm^{-2} (Fig. 5e). Furthermore, NCM811/d-PVDF/Li batteries exhibited excellent capacity retention of 94.9% after 300 cycles at 1C.

These findings underscore the potential of modifying PVDF to create fast ion-conducting pathways, achieving significant

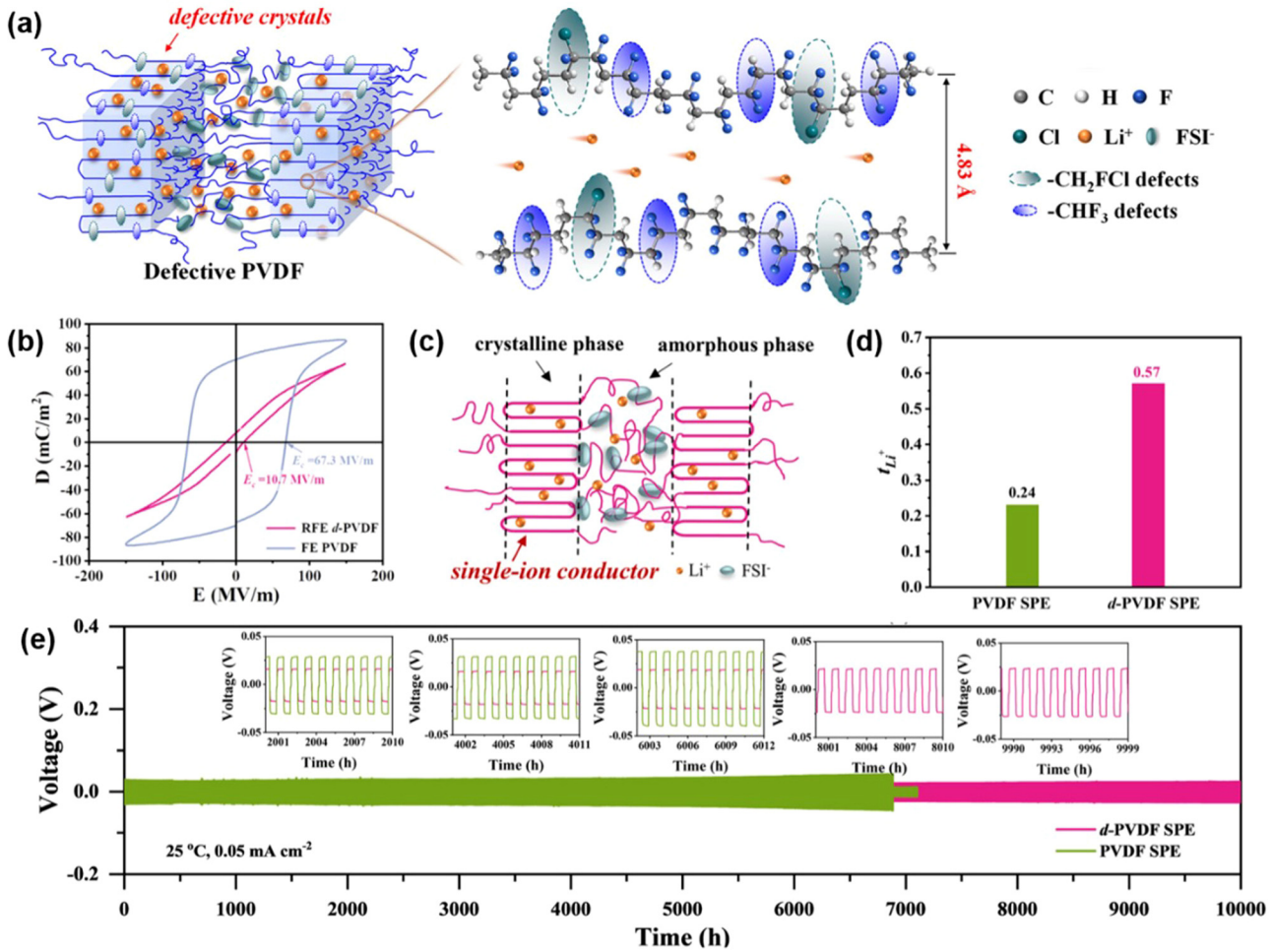

Fig. 5 Chemical modification of PVDF for enhanced PVDF-based SSE. (a) Schematic illustrating Li^+ transport within d-PVDF crystals. (b) Bipolar D–E loops of PVDF and d-PVDF. (c) Schematic representation of Li^+ and FSI^- location within d-PVDF SPE. (d) Lithium-ion transference number (t_{Li^+}) comparison between PVDF and d-PVDF SPE. (e) Cycling performance of Li//Li symmetrical cells with d-PVDF and PVDF SSE. Reproduced with permission.[69] Copyright 2024, Energy & Environmental Science.

improvements in ionic conductivity, lithium-ion transference, and overall stability in PVDF-based SSEs for advanced lithium metal batteries.

2.5 Other strategies

Beyond filler addition, constructing composite solid electrolytes (CSEs) with a ceramic body and a 3D-engineered scaffold infiltrated with a conductive polymer offers significant potential. This approach provides enhanced ionic transport, electrochemical stability, low interfacial resistance, and high mechanical strength. Wang *et al.* developed a conductive CSE featuring a cubic $Li_{6.1}Al_{0.3}La_3Zr_2O_{12}$ (LLZO) porous framework embedded in PVDF, forming a continuous 3D structure (Fig. 6a).[70] The formation of La–N and La–F bonds between the ceramic and polymer matrix aids Li salt dissociation, enabling efficient ion transport. These interactions led to a high ionic conductivity of 0.437 mS cm^{-1} and a lithium-ion transference number (t_{Li^+}) of 0.72 at 25 °C.

The ceramic skeleton creates a 3D conductive network with micron-sized pores that allow solubilized SSEs to permeate (Fig. 6b). The resulting SSE has high porosity (45.74%) and a wide voltage window (5.08 V), making it compatible with high-voltage cathodes. The ceramic-based SSE, with a high ceramic-mass composition (93%), provides robust mechanical support that suppresses lithium dendrite formation, while the porous LLZO framework allows for substantial PVDF-LiTFSI loading (Fig. 6c).

When used in LiNCM622/ceramic-based SSE/Li full solid-state lithium metal batteries (SSLMBs), the CSE demonstrated stable cycling over 200 times within a voltage range of 3 to 4.8 V, maintaining a high coulombic efficiency of 99.76% at 0.2C (Fig. 6d). After 200 cycles, the interfacial zone between the cathode and CSE remained intact, with no delamination or cracking. Additionally, an F^- and N-rich interface formed between the cathode and ceramic-based CSE, enhancing stability and performance (Fig. 6e). This 3D scaffold approach high-

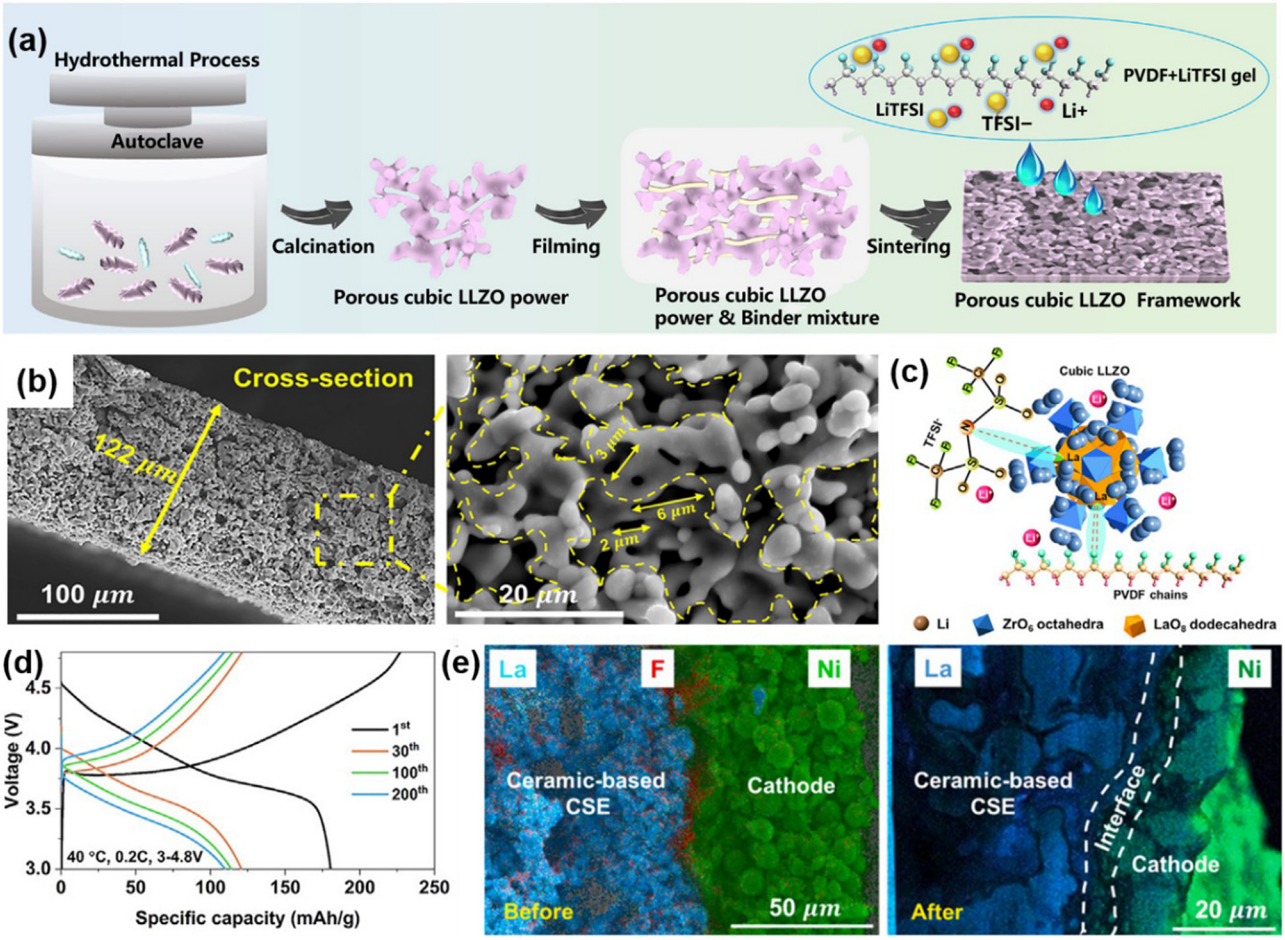

Fig. 6 Additional strategies for enhancing the performance of PVDF-based SSE. (a) Schematic illustration of ceramic-based CSE. (b) Cross-sectional SEM image and magnified view of the selected region of the CSE. (c) Illustration of the interactions between PVDF-LiTFSI CSE and porous LLZO framework. (d) Charge–discharge voltage profiles of a Li/ceramic-based CSE/NCM622 solid-state battery. (e) Cross-sectional SEM and corresponding EDS mappings of the SSB before and after cycling at 3–4.8 V. Reproduced with permission.[70] Copyright 2024, Cell Reports Physical Science.

lights the potential for creating stable, high-performance PVDF-based SSEs suitable for high-voltage and long-cycle SSLMB applications.

3. Conclusion and perspective

In summary, this review has highlighted the applications of PVDF-based SSEs in lithium metal anodes, covering strategies such as doping with inorganic fillers, blending with organic fillers, incorporating inorganic/organic composite fillers, modifying PVDF, and other approaches. Related fabrication methods, micro- and nanostructures, and electrochemical performance improvements have been systematically reviewed. These strategies have significantly enhanced the electrochemical performance of PVDF-based solid-state lithium metal batteries. However, several critical challenges remain for advancing PVDF-based SSEs to practical applications. Future studies may focus on the following areas:

3.1. Development of functional materials to modify PVDF-based SSEs

Current research mainly focuses on PVDF-based SSEs at low current densities and room temperatures. It is essential to develop PVDF-based SSEs with high thermal and electrochemical stability that can operate under elevated temperatures and higher current rates. Additionally, most modified fillers are limited to metal oxide electrolytes within PVDF matrices. Exploration of PVDF-based SSEs with sulfide and halide electrolytes is still limited, despite the superior ionic conductivity of sulfides. Combining PVDF-based SSEs with sulfide electrolytes could potentially improve SSLMB electrochemical performance.

3.2. In-depth mechanistic studies of PVDF-based SSEs in LMBs

Although considerable research has been conducted on PVDF-based SSE materials, theoretical calculations and mechanistic insights remain underexplored. Establishing a comprehensive

evaluation standard for PVDF-based SSEs in LMBs is crucial for future material advancements. Advanced operando techniques, such as *in situ* X-ray diffraction (XRD), scanning electron microscopy (SEM), transmission electron microscopy (TEM), and nuclear magnetic resonance (NMR), are essential for real-time insights into ion transport during the charging/discharging process. Integrating theoretical calculations (*e.g.*, DFT calculations, molecular dynamics simulations) with *in situ* characterization techniques is urgently needed to understand surface and interfacial chemistry and physics changes during cycling.

3.3. Development of thin PVDF-based SSEs with high mechanical strength

Current PVDF-based SSEs typically have thicknesses around 100 μm, limiting their potential to enhance energy density. Thinner electrolytes (10–20 μm) are essential for achieving higher energy density in SSLMBs. At the same time, these thinner electrolytes must possess sufficient mechanical strength to prevent lithium dendrite penetration, which may require incorporating inorganic materials. To support high-loading cathodes, combining cathode materials with solid electrolytes could be a viable solution.

3.4. Bridging the gap between research and practical applications

The development of 300 W h kg^{-1} pouch cells represents a significant advancement in SSLMBs, positioning them closer to commercial viability. Pouch cells hold the potential to further elevate SSLMB energy densities to 500 W h kg^{-1}, which could expedite their industrialization and application in daily life. The production of PVDF-based lithium metal pouch cells has a promising future, although numerous unknown challenges still need to be addressed.

In conclusion, this review provides a foundational understanding and recent advancements in the design and use of PVDF-based SSEs for SSLMBs. It will inform future efforts in developing high-performance PVDF-based SSLMBs and help accelerate their practical applications.

Data availability

No primary research results, software or code have been included and no new data were generated or analyzed as part of this review.

Conflicts of interest

There are no conflicts to declare.

Acknowledgements

Z. L. and G. X. acknowledge the support of National Key Research and Development Program of China (2022YFB3803502), National Natural Science Foundation of China (52103076), and Shanghai Rising-Star Program (24QA2700100). M. S. I. and C. C. thank the support of USDA-NIFA (Grant No. 2021-67021-33998) and Case Western Reserve University.

References

1 C. Dang, Y. Cao, H. Nie, W. Lang, J. Zhang, G. Xu and M. Zhu, *Nat. Water*, 2024, **2**, 115–126.
2 A. Olabi and M. A. Abdelkareem, *Renewable Sustainable Energy Rev.*, 2022, **158**, 112111.
3 Y. Pang, Y. Cao, M. Derakhshani, Y. Fang, Z. L. Wang and C. Cao, *Matter*, 2021, **4**, 116–143.
4 Y. Pang, Y. Fang, J. Su, H. Wang, Y. Tan and C. Cao, *Adv. Mater. Technol.*, 2023, **8**, 2201246.
5 Y. Pang, Z. Huang, Y. Fang, X. Xu and C. C. Cao, *Nano Energy*, 2023, **114**, 108659.
6 X. Zhu, Z. Xu, T. Zhang, J. Zhang, Y. Guo, M. Shan, K. Wang, T. Shi, G. Cui, F. Wang, G. Xu and M. Zhu, *Adv. Funct. Mater.*, 2024, **34**, 2407262.
7 S. Chen, M. Zhang, P. Zou, B. Sun and S. Tao, *Energy Environ. Sci.*, 2022, **15**, 1805–1839.
8 J. Xu, X. Cai, S. Cai, Y. Shao, C. Hu, S. Lu and S. Ding, *Energy Environ. Mater.*, 2023, **6**, e12450.
9 Y. Pang, Y. Cao, Y. Chu, M. Liu, K. Snyder, D. MacKenzie and C. Cao, *Adv. Funct. Mater.*, 2020, **30**, 1906244.
10 S. Chae, S. H. Choi, N. Kim, J. Sung and J. Cho, *Angew. Chem., Int. Ed.*, 2020, **59**, 110–135.
11 B. Liu, J.-G. Zhang and W. Xu, *Joule*, 2018, **2**, 833–845.
12 B. Jagger and M. Pasta, *Joule*, 2023, **7**, 2228–2244.
13 Z. X. Liu, S. H. Ha, Y. Liu, F. Wang, F. Tao, B. R. Xu, R. H. Yu, G. X. Wang, F. Z. Ren and H. X. Li, *J. Mater. Sci. Technol.*, 2023, **133**, 165–182.
14 X. Yang, Q. Yin, C. Wang, K. Doyle-Davis, X. Sun and X. Li, *Prog. Mater. Sci.*, 2023, **140**, 101193.
15 J. Wang, B. Ge, H. Li, M. Yang, J. Wang, D. Liu, C. Fernandez, X. Chen and Q. Peng, *Chem. Eng. J.*, 2021, **420**, 129739.
16 S. Y. Yuan, T. Y. Kong, Y. Y. Zhang, P. Dong, Y. J. Zhang, X. L. Dong, Y. G. Wang and Y. Y. Xia, *Angew. Chem., Int. Ed.*, 2021, **60**, 25624–25638.
17 Z. Liu, Y. Liu, Y. Miao, G. Liu, R. Yu, K. Pan, G. Wang, X. Pang and J. Ma, *Energy Environ. Mater.*, 2023, **6**, e12525.
18 Y. Lin, S. Huang, L. Zhong, S. Wang, D. Han, S. Ren, M. Xiao and Y. Meng, *Energy Storage Mater.*, 2021, **34**, 128–147.
19 F. Liang, Y. L. Sun, Y. F. Yuan, J. Huang, M. J. Hou and J. Lu, *Mater. Today*, 2021, **50**, 418–441.
20 J. Wu, S. Liu, F. Han, X. Yao and C. Wang, *Adv. Mater.*, 2021, **33**, 2000751.
21 P. Hagenmuller and W. Van Gool, *Solid electrolytes: general principles, characterization, materials, applications*, Elsevier, 2013.

22 T. Ye, L. Li and Y. Zhang, *Adv. Funct. Mater.*, 2020, **30**, 2000077.
23 Z. Y. Wang, L. Shen, S. G. Deng, P. Cui and X. Y. Yao, *Adv. Mater.*, 2021, **33**, 2100353.
24 J. C. Bachman, S. Muy, A. Grimaud, H. H. Chang, N. Pour, S. F. Lux, O. Paschos, F. Maglia, S. Lupart, P. Lamp, L. Giordano and Y. Shao-Horn, *Chem. Rev.*, 2016, **116**, 140–162.
25 Q. Zheng, Y. Song, W. Huang, J. Yang, T. Li and Y. Xu, *Energy Storage Mater.*, 2023, **63**, 103038.
26 S. Kalnaus, N. J. Dudney, A. S. Westover, E. Herbert and S. Hackney, *Science*, 2023, **381**, 1300.
27 Y. M. Jin, Q. S. He, G. Z. Liu, Z. Gu, M. Wu, T. Y. Sun, Z. H. Zhang, L. F. Huang and X. Y. Yao, *Adv. Mater.*, 2023, **35**, 2211047.
28 P. Jiang, G. Du, J. Cao, X. Zhang, C. Zou, Y. Liu and X. Lu, *Energy Technol.*, 2023, **11**, 2201288.
29 Q. Zhang, D. Cao, Y. Ma, A. Natan, P. Aurora and H. Zhu, *Adv. Mater.*, 2019, **31**, 1901131.
30 Z. H. Zhang, L. P. Wu, D. Zhou, W. Weng and X. Y. Yao, *Nano Lett.*, 2021, **21**, 5233–5239.
31 M. L. Yang, Y. Yao, M. Y. Chang, F. L. Tian, W. R. Xie, X. L. Zhao, Y. Yu and X. Y. Yao, *Adv. Energy Mater.*, 2023, **13**, 2300962.
32 L. Hu, X. Gao, H. Wang, Y. Song, Y. Zhu, Z. Tao, B. Yuan and R. Hu, *Small*, 2024, 2312251.
33 Z. H. Jia, Y. Liu, H. M. Li, Y. Xiong, Y. J. Miao, Z. X. Liu and F. Z. Ren, *J. Energy Chem.*, 2024, **92**, 548–571.
34 Y. Gong, C. Wang, M. Xin, S. Chen, P. Xu, D. Li, J. Liu, Y. Wang, H. Xie, X. Sun and Y. Liu, *Nano Energy*, 2023, **119**, 109054.
35 Y. Wu, Y. Li, Y. Wang, Q. Liu, Q. Chen and M. Chen, *J. Energy Chem.*, 2022, **64**, 62–84.
36 F. Liu, N. A. Hashim, Y. Liu, M. M. Abed and K. Li, *J. Membr. Sci.*, 2011, **375**, 1–27.
37 X. Zhang, S. Wang, C. J. Xue, C. Z. Xin, Y. H. Lin, Y. Shen, L. L. Li and C. W. Nan, *Adv. Mater.*, 2019, **31**, 1806082.
38 X. Zhang, S. Wang, C. Xue, C. Xin, Y. Lin, Y. Shen, L. Li and C.-W. Nan, *Adv. Mater.*, 2020, **32**, 2000026.
39 X. Zhang, T. Liu, S. Zhang, X. Huang, B. Xu, Y. Lin, B. Xu, L. Li, C.-W. Nan and Y. Shen, *J. Am. Chem. Soc.*, 2017, **139**, 13779–13785.
40 L. Liu, D. C. Zhang, J. W. Zhao, J. D. Shen, F. K. Li, Y. Yang, Z. B. Liu, W. X. He, W. M. Zhao and J. Liu, *ACS Appl. Energy Mater.*, 2022, **5**, 2484–2494.
41 Y. Ma, C. Wang, K. Yang, B. Li, Y. Li, S. Guo, J. Lv, X. An, M. Liu, Y.-B. He and F. Kang, *ACS Appl. Mater. Interfaces*, 2023, **15**, 17978–17985.
42 X. An, Y. Liu, K. Yang, J. Mi, J. Ma, D. Zhang, L. Chen, X. Liu, S. Guo, Y. Li, Y. Ma, M. Liu, Y.-B. He and F. Kang, *Adv. Mater.*, 2024, **36**, 2311195.
43 Y. Wu, H. Zhang, Y. Xu, Z. Tang and Z. Li, *J. Mater. Chem. A*, 2024, **12**, 20403–20413.
44 T. Pareek, S. Dwivedi, S. A. Ahmad, M. Badole and S. Kumar, *J. Alloys Compd.*, 2020, **824**, 153991.
45 X. Bai, G. Zhao, G. Yang, M. Wang, J. Zhang and N. Zhang, *Energy Storage Mater.*, 2023, **63**, 103041.
46 X. Song, T. Zhang, S. Huang, J. Mi, Y. Zhang, J. Travas-Sejdic, A. P. Turner, W. Gao and P. Cao, *J. Power Sources*, 2023, **564**, 232849.
47 F. Liu, L. Gao, Z. Zhang, L. Zhang, N. Deng, Y. Zhao and W. Kang, *Energy Storage Mater.*, 2024, **64**, 103072.
48 W. Yang, Y. Liu, X. Sun, Z. He, P. He and H. Zhou, *Angew. Chem., Int. Ed.*, 2024, **63**, e202401428.
49 P. Yao, B. Zhu, H. Zhai, X. Liao, Y. Zhu, W. Xu, Q. Cheng, C. Jayyosi, Z. Li, J. Zhu, K. M. Myers, X. Chen and Y. Yang, *Nano Lett.*, 2018, **18**, 6113–6120.
50 B. Li, Q. Su, L. Yu, D. Wang, S. Ding, M. Zhang, G. Du and B. Xu, *ACS Appl. Mater. Interfaces*, 2019, **11**, 42206–42213.
51 P. R. Shi, J. B. Ma, M. Liu, S. K. Guo, Y. F. Huang, S. W. Wang, L. H. Zhang, L. K. Chen, K. Yang, X. T. Liu, Y. H. Li, X. F. An, D. F. Zhang, X. Cheng, Q. D. Li, W. Lv, G. M. Zhong, Y. B. He and F. Y. Kang, *Nat. Nanotechnol.*, 2023, **18**, 602–610.
52 T. S. Feng, Y. B. Hu, L. Xu, J. Q. Huang, S. B. Hu, L. F. Zhang and L. L. Luo, *Mater. Today Energy*, 2022, **28**, 101062.
53 S. Lv, X. He, Z. Ji, S. Yang, L. Feng, X. Fu, W. Yang and Y. Wang, *Adv. Energy Mater.*, 2023, **13**, 2302711.
54 R. Orenstein, Z. Li, M. Dirican, H. Cheng, L. Chang, M. Yanilmaz, C. Yan and X. Zhang, *ACS Appl. Mater. Interfaces*, 2024, **16**, 33428–33438.
55 L. K. Chen, T. Gu, J. B. Ma, K. Yang, P. R. Shi, J. Biao, J. S. Mi, M. Liu, W. Lv and Y. B. He, *Nano Energy*, 2022, **100**, 107470.
56 Y. Liang, J. Zhang, S. Guan, K. Wen, C. Guo, Y.-H. Wu, H. Yuan, S. Liu, Y. Qi, W. Mo, X. Zhang and C. W. Nan, *J. Materiomics*, 2024, **10**, 880–888.
57 S. Zhang, H. Liu, Z. Liu, Y. Zhao, J. Yan, Y. Zhang, F. Liu, Q. Liu, C. Liu, G. Sun, Z. Wang, J. Yang and Y. Ren, *Adv. Funct. Mater.*, 2024, **34**, 2401377.
58 Y. Zhao, Y. Qin, X. Da, X. Weng, Y. Gao, G. Gao, Y. Su and S. Ding, *ChemSusChem*, 2022, **15**, e202201554.
59 C. Xue, X. Zhang, S. Wang, L. Li and C.-W. Nan, *ACS Appl. Mater. Interfaces*, 2020, **12**, 24837–24844.
60 S. Guan, K. Wen, Y. Liang, C. Xue, S. Liu, J. Yu, Z. Zhang, X. Wu, H. Yuan, Z. Lin, H. Yu, L. Li and C.-W. Nan, *J. Mater. Chem. A*, 2022, **10**, 24269–24279.
61 Y. Hu, L. Liu, J. Zhao, D. Zhang, J. Shen, F. Li, Y. Yang, Z. Liu, W. He, W. Zhao and J. Liu, *Batteries*, 2023, **9**, 322.
62 X. Y. Hu, K. L. Liu, S. J. Zhang, G. S. Shao, S. R. P. Silva and P. Zhang, *Nano Res.*, 2023, **17**, 2824–2835.
63 X. Li, Y. Wang, Q. Zhou, H. Kuai, C. Ji and X. Xiong, *J. Mater. Chem. A*, 2024, **12**, 7645–7653.
64 L. Yang, Y. Mu, L. Zou, C. Li, Y. Feng, Y. Chu, D. Zuo, S. Das, L. Wei, Q. Zhang, J. Wan and L. Zeng, *Nano Lett.*, 2024, **24**, 13162–13171.
65 Y. T. Ma, Y. Qiu, K. Yang, S. Lv, Y. H. Li, X. F. An, G. Y. Xiao, Z. Han, Y. T. Ma, L. K. Chen, D. F. Zhang, W. Lv, Y. Tian, T. Z. Hou, M. Liu, Z. Zhou, F. Y. Kang and Y. B. He, *Energy Environ. Sci.*, 2024, **17**, 8274–8283.
66 K. Fan, X. Lai, Z. Zhang, L. Chai, Q. Yang, G. He, S. Liu, L. Sun, Y. Zhao, Z. Hu and L. Wang, *J. Power Sources*, 2023, **580**, 233342.

67 Y. Liang, L. Dong, S. Zhong, B. Yuan, Y. Dong, Y. Liu, C. Yang, D. Tang, J. Han and W. He, *Mater. Today Phys.*, 2021, **21**, 100554.
68 Q. Zeng, D. Zhu, J. Shan, Q. Gao, J. Xu, Q. Xu, P. Shi and Y. Min, *Chem. Eng. J.*, 2024, **486**, 150189.
69 C. Dai, M. Weng, B. Cai, J. Liu, S. Guo, H. Xu, L. Yao, F. J. Stadler, Z. M. Li and Y. F. Huang, *Energy Environ. Sci.*, 2024, **17**, 8243–8253.
70 S. Wang, S. Bessette, R. Gauvin and G. P. Demopoulos, *Cell Rep. Phys. Sci.*, 2024, **5**, 102213.
71 B. Cheng, P. Du, J. Xiao, X. Zhan and L. Zhu, *ACS Appl. Mater. Interfaces*, 2024, **16**, 31648–31656.
72 Y. F. Huang, T. Gu, G. Rui, P. Shi, W. Fu, L. Chen, X. Liu, J. Zeng, B. Kang, Z. Yan, F. J. Stadler, L. Zhu, F. Kang and Y. B. He, *Energy Environ. Sci.*, 2021, **14**, 6021–6029.
73 Q. Zhu, T. Zhang, X. Zhu, J. Zhang, M. Shan, Z. Hu, G. Xu and M. Zhu, *Energy Mater.*, 2024, **4**, 400016.
74 P. R. Shi, J. B. Ma, M. Liu, S. K. Guo, Y. F. Huang, S. W. Wang, L. H. Zhang, L. K. Chen, K. Yang, X. T. Liu, Y. H. Li, X. F. An, D. F. Zhang, X. Cheng, Q. D. Li, W. Lv, G. M. Zhong, Y. B. He and F. Y. Kang, *Nat. Nanotechnol.*, 2023, **18**, 602.
75 L. K. Chen, T. Gu, J. B. Ma, K. Yang, P. R. Shi, J. Biao, J. S. Mi, M. Liu, W. Lv and Y. B. He, *Nano Energy*, 2022, **100**, 107470.